

# Platinum Nanoparticles to Enable Electrodynamic Therapy for Effective Cancer Treatment

Tongxu Gu, Yao Wang, Yunhao Lu, Liang Cheng, Liangzhu Feng, Hui Zhang, Xiang Li,\*  
Gaorong Han,\* and Zhuang Liu\*

**Electrochemical therapy (EChT), by inserting electrodes directly into tumors to kill cancer cells under direct current (DC), is clinically used in several countries. In EChT, the drastic pH variation nearby the inserted electrodes is the main cause of tumor damage. However, its limited effective area and complex electrode configuration have hindered the clinical application of EChT in treating diverse tumor types. Herein, a conceptually new electric cancer treatment approach is presented through an electro-driven catalytic reaction with platinum nanoparticles (PtNPs) under a square-wave alternating current (AC). The electric current triggers a reaction between water molecules and chloride ions on the surface of the PtNPs, generating cytotoxic hydroxyl radicals. Such a mechanism, called electrodynamic therapy (EDT), enables effective killing of cancer cells within the whole electric field, in contrast to EChT, which is limited to areas nearby electrodes. Remarkable tumor destruction efficacy is further demonstrated in this *in vivo* EDT treatment with PtNPs. Therefore, this study presents a new type of cancer therapy strategy with a tumor-killing mechanism different from existing methods, using nanoparticles with electrocatalytic functions. This EDT method appears to be minimally invasive, and is able to offer homogeneous killing effects to the entire tumor with a relatively large size.**

Electrochemical therapy (EChT) utilizes destructive electrolysis induced by low-voltage direct current (DC) passing through two or more electrodes inserted into the tumor to destruct solid tumors. Over years, EChT has been used clinically to ablate solid tumors in some countries, mainly in China and Germany.<sup>[1]</sup> During EChT, electrolysis is initiated by electro-osmosis due to water migration from the anode to the cathode, causing

dryness in tissue surrounding the anode and edema at the cathode.<sup>[2]</sup> The mechanism of EChT-induced tumor destruction, which has been proven theoretically<sup>[3]</sup> and experimentally,<sup>[4]</sup> is known to be related to the drastic pH changes around the electrodes without heating effect. There are also studies indicating that reactive oxygen species (ROS) produced around the electrodes would also be responsible for cell killing during EChT.<sup>[5]</sup> EChT has relatively localized destruction region and less side effects compared to other systemic treatment, and is particularly suitable for eliminating non-resectable tumors as a relatively inexpensive technique.<sup>[6]</sup> However, it must be noted that EChT is not a selective treatment method and would destroy normal cells together with tumor cells. Besides, when tumors have abnormal shapes or large sizes, more than two electrodes need to be adopted in the EChT.<sup>[7]</sup> Such multiple insertion of electrodes not only complicates the clinical operations, but also leads to extra discomfort and pain to patients.<sup>[8]</sup> Till now,

disputes on the standardization of electrode displacement and therapeutic dose stay controversial and remain challenging.<sup>[9]</sup>

In recent years, considerable effort has been devoted to the development of ROS-based cancer treatment strategies.<sup>[10]</sup> Representative approaches include photodynamic therapy (PDT),<sup>[11]</sup> sonodynamic therapy (SDT),<sup>[12]</sup> as well as recently proposed chemodynamic therapy (CDT)<sup>[13]</sup> and radiodynamic therapy (RDT).<sup>[14]</sup> In those methods, the generation of ROS is triggered by either exogenous energy input such as laser, ultrasound, and ionizing irradiation, or endogenous chemical energy such as intratumoral H<sub>2</sub>O<sub>2</sub>. ROS generated during such treatment possesses the ability to cause apoptosis or necrosis by damaging cellular constituents of cancer cells (e.g., lipids, proteins, and DNA).<sup>[15]</sup> To enable or enhance those “dynamic therapies,” nanoparticles (NPs) with small sizes, large surface areas, and abundant surface defects are often employed as therapeutic agents with catalytic activities to facilitate the generation of ROS.<sup>[16]</sup> However, the possibility of combining nanotechnology with electronic current to realize efficient cancer therapy has not yet been explored to the best of our knowledge.

Herein, we present a new conceptual approach for cancer treatment, namely “electrodynamic therapy (EDT),” utilizing

T. X. Gu, Y. Wang, Dr. Y. H. Lu, Prof. H. Zhang, Dr. X. Li, Prof. G. R. Han  
State Key Laboratory of Silicon Materials  
School of Materials Science and Engineering  
Zhejiang University  
Hangzhou, Zhejiang 310027, P. R. China  
E-mail: xiang.li@zju.edu.cn; hgr@zju.edu.cn  
Dr. L. Cheng, Dr. L. Feng, Prof. Z. Liu  
Institute of Functional Nano & Soft Materials (FUNSOM)  
Jiangsu Key Laboratory for Carbon-Based Functional Materials & Devices  
Soochow University  
Suzhou 215123, P. R. China  
E-mail: zliu@suda.edu.cn

 The ORCID identification number(s) for the author(s) of this article can be found under <https://doi.org/10.1002/adma.201806803>.

DOI: 10.1002/adma.201806803

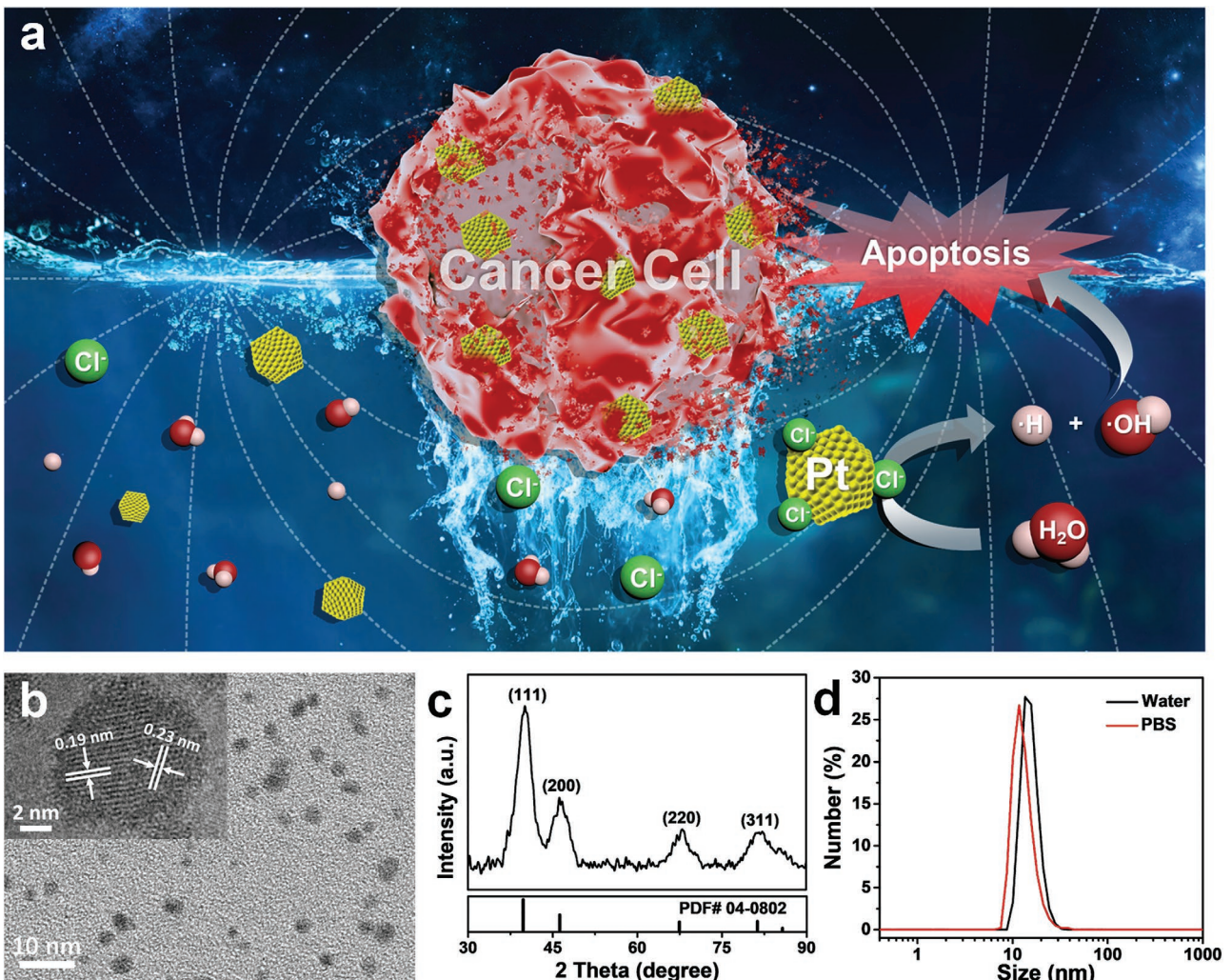


**Figure 1.** PtNPs for EDT. a) Schematic illustration of electrodynamic cancer therapy. b) A TEM image of PtNPs, inset: a high-magnification TEM image. c) XRD spectrum of as-made PtNPs. d) DLS measured sizes of PtNPs dissolved in water and PBS.

the electro-driven catalytic reaction occurred on platinum nanoparticles (PtNPs) under the square-wave alternating current (AC) electric field. PtNPs have been extensively reported as nanozymes with tailored catalytic activity and ROS scavenging agent in recent years.<sup>[17]</sup> Many studies have also demonstrated the biocompatibility of PtNPs.<sup>[18]</sup> In our study, under the action of an electric field, the Faraday cage effect occurs on the surface of PtNPs and produces a hole-doping condition. Dissociation reaction of water molecules occurs subsequently, generating cytotoxic hydroxyl radicals ( $\cdot\text{OH}$ ) with the assist of chlorine ions (Figure 1a). As the results, cancer cells incubated with PtNPs could be effectively killed under square-wave AC field, which unlikely DC field used EChT would not cause significant pH changes nearby electrodes. In vivo EDT is then realized through this electro-driven catalytic reaction just by applying square-wave AC on tumors injected with PtNPs, achieving rather effective therapeutic effect to eliminate tumors with large sizes (over  $500 \text{ mm}^3$ ). This work thus presents a nanotechnology-based EDT strategy as a new type of cancer treatment method with high potency and minimal invasiveness.

Well-dispersed PtNPs were prepared by a facile chemical reduction method,<sup>[19]</sup> with polyvinylpyrrolidone (PVP) as a stabilizing agent and  $\text{NaBH}_4$  as a reducing agent at ambient temperature. As observed by transmission electron microscopy (TEM), the obtained PtNPs showed homogeneous size distribution (Figure 1b). Under high-resolution TEM imaging (Figure 1b, inset), crystalline fringes with interplanar spacings of 0.19 and 0.23 nm correspond to the (200) and (111) plane of the face-centered cubic Pt (JCPDS PDF#04-0802), respectively. The X-ray diffraction (XRD) analysis further confirmed these results (Figure 1c). With PVP coating, as-prepared PtNPs showed great solubility in aqueous solutions including water, phosphate buffer solution (PBS), fetal bovine serum (FBS), and RPMI-1640 cell culture medium (Figure S1, Supporting Information). As determined by dynamic light scattering (DLS), PtNPs presented a mean hydrodynamic diameter of  $\approx 15 \text{ nm}$ , which remained constant in PBS (Figure 1d). The  $\zeta$  potential of those PtNPs was determined to be  $-0.08 \text{ mV}$ , which was almost neutral, suggesting that those nanoparticles would barely be driven to move by the electric field in the following experiment.

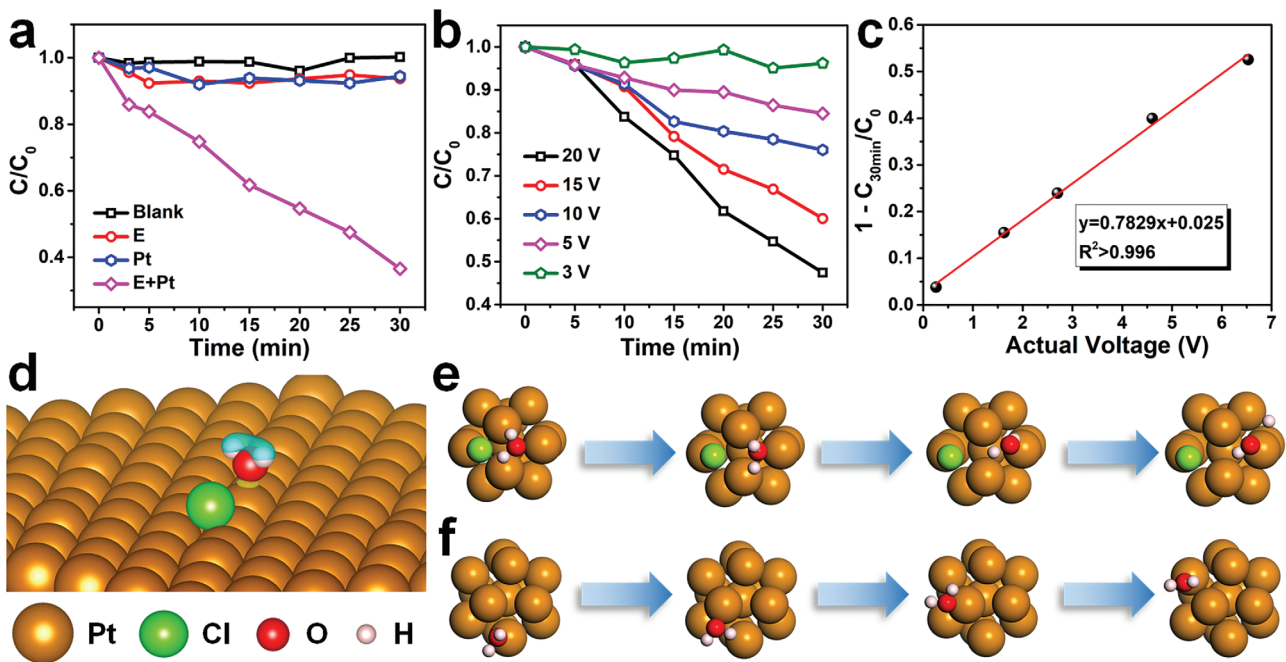


**Figure 2.** The electro-driven catalytic performance. a) Degradation rates of MB under different conditions ([Pt]: 100  $\mu\text{g mL}^{-1}$ , DC output voltage: 20 V, [MB]:  $0.03 \times 10^{-3}$  M). b) Effect of the output voltage on the degradation of MB. c) The relationship between actual voltage and the degradation of MB. d) Initial state of differential charge density diagram on platinum surface absorbed by water molecule and chloride atom. Yellow and blue colors represent the charge accumulation and depletion regions, respectively. e,f) Diagram of H<sub>2</sub>O molecule absorbed on Pt-cluster surface process through molecular dynamics simulation with or without chloride atom.

Methylene blue (MB) is a blue cationic thiazine dye often used to detect the generation of hydroxyl free radicals ( $\cdot\text{OH}$ ),<sup>[20]</sup> which can react with MB, resulting in diminished color for the MB solution. In our work, the electro-driven catalytic activity of PtNPs was evaluated by using MB as the ROS probe in a double salt bridge system (Figure S2, Supporting Information). As shown in Figure 2a, the absorption intensity of MB (at 664 nm) in PBS gradually decreased in the presence of PtNPs and DC power supply. Conversely, there was no clear degradation in the groups of control, PtNPs only, and DC power supply only. Similar phenomena were also observed in RPMI-1640 cell culture medium (Figure S3, Supporting Information). After calibrating the actual voltage across the closest ends of salt bridges as well as the current follow against the output voltage of the power supply (Figure S4, Supporting Information), we studied the voltage-dependent MB degradation behaviors in the same system (Figure 2b). Notably, the degree of MB degradation showed linear dependence with the actual voltage in the presence of PtNPs (Pt concentration = 100  $\mu\text{g mL}^{-1}$ ) (Figure 2c). The other three noble metal (Au, Ir, and Pd) nanoparticles with similar diameters and the same weight concentration were also used in this electro-driven catalytic degradation experiment (Figure S5, Supporting Information). Except for Au nanoparticles, Pd and Ir nanoparticles could also trigger the degradation of MB under DC power supply. According to the d-band center theory, this is related to the unfilled d orbital of Pd, Pt, and Ir, which facilitates the formation of coordination bonds to participate in catalytic reaction. However, Au has a filled d band and stable electronic structure, thus is not effective in this process.<sup>[21]</sup> With the highest activity, PtNPs were chosen in our following investigations.

The mechanism of the electric-current-triggered ROS production by PtNPs was further investigated. Interestingly, we found that the existence of Cl<sup>-</sup> ions in the solution is critical to the MB degradation triggered by PtNPs under electric current (Figure S6, Supporting Information). In the absence of Cl<sup>-</sup> ions, the PtNP-triggered degradation of MB under the same DC appeared to be much slower. We thus speculated that chloride ions played a vital role in this system.

To further confirm results that we discussed above, first-principle calculations were performed to study chlorine adsorption and water dissociation on the most stable low-index face Pt (111).<sup>[22]</sup> First, we investigated the adsorption site of chlorine ions on Pt (111). As a result, Cl<sup>-</sup> ions are favorable to adsorb on face-centered cubic (Fcc) sites of Pt (111) surface, in good agreement with the previous work.<sup>[22]</sup> Second, we examined water molecular dissociation reaction in the process. Hole-doping condition was taken into consideration to simulate the Faraday cage effect of conductor PtNPs under the electric field. Neutral condition was used as a control. The initial step of the water dissociation reaction was shown in Figure 2d. H<sub>2</sub>O molecules and Cl<sup>-</sup> ions were both adsorbed on the Pt (111) surface in a neutral environment. To explore the inherent mechanism of this reaction, we plotted differential charge density ( $\Delta\rho$ ) for the system. The differential charge density is defined as  $\Delta\rho = \rho - \rho_{\text{H}_2\text{O}} - \rho_{\text{Cl}^-\text{Pt}}$ , where  $\rho$  is total charge density of the whole slab,  $\rho_{\text{H}_2\text{O}}$  is the charge density of the water molecular, and  $\rho_{\text{Cl}^-\text{Pt}}$  is the charge density of the Pt (111) surface with Cl<sup>-</sup> ions. Figure 2d shows the charge transfer between H<sub>2</sub>O molecule and Pt surface, with the yellow and blue colors representing the charge accumulation and depletion regions, respectively. We observed charge reduction on H atom

whereas charge accumulated on Pt atoms around the oxygen atom. Starting from neutral environment, when we increased the concentration of hole doping, the charge reduction on H atom was even more obvious. At the same time, the H–O bond length increased, showing a tendency to form hydroxyl groups as displayed in Figure S7 (Supporting Information). The loss of charge on H atoms was increased in the cases of hole doping. Nevertheless, charge transferred from Pt surface to Cl<sup>-</sup> ions resulting from electronegativity difference.

In order to exclude the possible errors due to periodic boundary condition, molecular dynamics (MD) simulations were investigated by DMol approach with nonperiodic condition.<sup>[23]</sup> The H<sub>2</sub>O molecule dissociation reaction process was performed with and without Cl<sup>-</sup> ion absorbed on Pt cluster (Figure 2e,f). In terms of the results, the H<sub>2</sub>O molecule was decomposed in the presence of Cl<sup>-</sup> ions, whereas the H–O bond did not break without Cl<sup>-</sup> ions. Therefore, this suggests that Cl<sup>-</sup> ions are the dominant driving force of water dissociation under electronic current on the surface of PtNPs.

Although dissociation reaction of water molecules could be catalyzed by PtNPs under the DC electric field, the electrolysis reaction products (H<sup>+</sup>, H<sub>2</sub>, O<sub>2</sub>, Cl<sub>2</sub>, OH<sup>-</sup>, etc.) on the electrodes have considerable damage to the biological tissue when the electric current is continuously applied. In contrast, these harmful electrolysis products instantly produced nearby electrodes could be neutralized under AC. The ions segregation caused by DC electric field driving in the solution would be reduced at the same time. Therefore, for better utilizing this performance in oncotherapy, we then tried square-wave AC power source in the following experiments. By changing the current duration time to 1, 10, 30, 60 s, and infinite (namely DC), the square-wave output waveforms were shown in Figure 3a. At the interval between each positive/negative switches, the output voltage returned to zero in 1 s. To control the same amount of electricity

flowing through the system, total effective time was used in the following experiment. After 10 min electrification in a double salt bridges device, pH changes of PBS solution in the container where the two electrodes were placed were recorded by pH test paper (Figure 3b). Comparing with the standard color chart, the pH value of the solution near the electrodes showed no significant change under square-wave AC power supply, while DC resulted in drastic pH change into extremely acidic nearby anode and extremely alkaline nearby cathode.

We then checked MB degradation behaviors on different square-wave AC treatments (Figure 3c; Figure S8, Supporting Information). Compared to the sample under the DC field, the MB degradation was found to be slower as the shortening of the current duration time under the square-wave AC field. According to this result, we speculated that changing the direction of electric field would affect the location of hole-doping area on the surface of PtNPs. In addition, the mass transfer of ions in PBS and the recombination of radicals would also influence the catalytic reaction process. Notably, for the sample treated by a 60 s square-wave AC field, which resulted in little pH fluctuation nearby electrodes, the MB degradation appeared to be similar compared to that achieved under the DC field. In addition to MB, 2-[6-(4-amino)phenoxy]-3*H*-xanthene-3-on-9-ylbenzoic acid (APF), a selective fluorescence probe to detect hydroxyl radicals (·OH) was also used in our work to evaluate the electronic current-induced ROS production triggered by PtNPs (Figure 3d).<sup>[24]</sup> Similarly, effective generation of ·OH as evidenced by the increased APF fluorescence was observed for samples containing PtNPs, in the presence of either DC field or 60 s square-wave AC field. Our data collectively suggest that PtNPs could act as an effective catalyst to produce ROS under electronic current, while the square-wave AC field with 60 s exchange could be the optimal condition for the subsequent EDT experiment. To confirm that the production of ·OH is

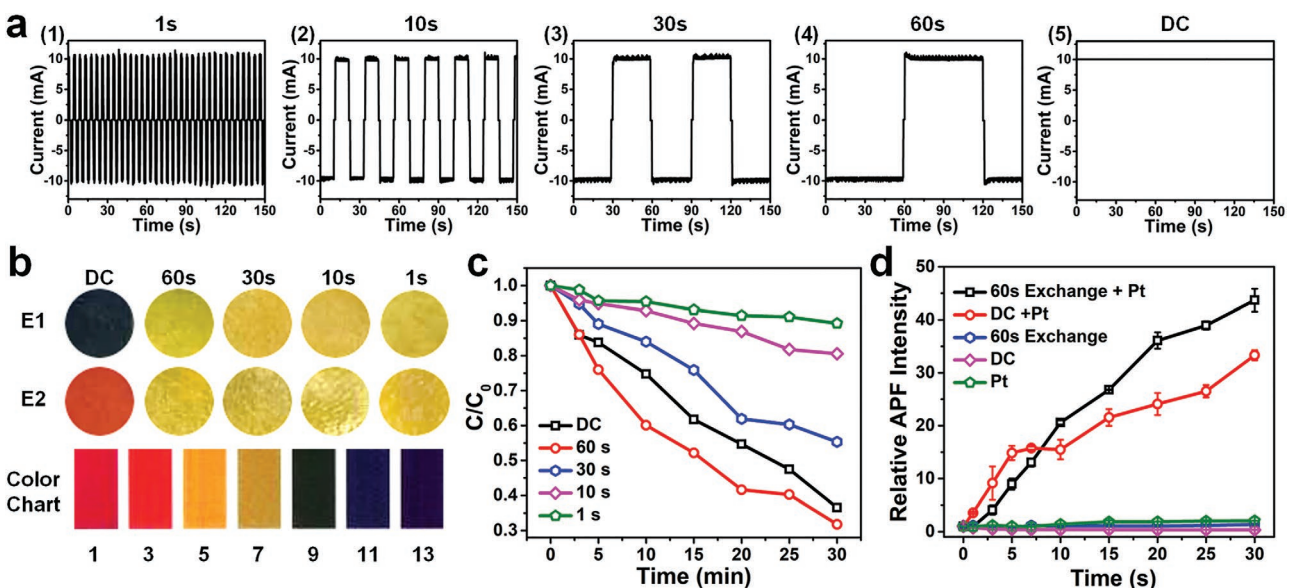


**Figure 3.** The electro-driven catalytic performance under square-wave AC. a) Square-wave output waveform with the current duration at 1, 10, 30, and 60 s, and infinite (namely DC). b) pH changes of PBS near the two electrodes after 10 min of electrification. c) Degradation rates of MB under square-wave AC field with different current durations or DC field in the presence of PtNPs ( $100 \mu\text{g mL}^{-1}$ ). d) Changes of APF fluorescence in absence and presence of PtNPs ( $100 \mu\text{g mL}^{-1}$ ) under 60 s square-wave AC or DC power source (output voltage: 20 V).

related to PtNPs, we studied MB degradation behaviors on different concentrations of PtNPs under 60 s AC field. As shown in Figure S9 (Supporting Information), the MB degradation rate was remarkably accelerated with the increased concentration of PtNPs. To further demonstrate the role of chloride ions in a square-wave AC system, we studied the electro-driven catalytic performance in KCl solutions with different concentrations under the 60 s AC field (Figure S10, Supporting Information). Notably, the MB degradation was found to be markedly accelerated as the increased concentrations of  $\text{Cl}^-$  ions in the electrolyte. When the concentration of KCl was greater than 0.3 M, the degree of MB degradation did not change further, implying that required chloride ions have reached a saturation level for this catalytic reaction. In addition, infrared (IR) spectra of PtNPs in PBS before and after the treatment by 60 s square-wave AC field for 30 min were recorded (Figure S11, Supporting Information). For the PtNP sample after AC treatment, the clear redshift of the IR peak at  $696\text{ cm}^{-1}$  and the decrease in peak strength at  $2079\text{ cm}^{-1}$  were consistent with the conclusion in the computational model (see the Supporting Information for the detailed explanation). The examination using electron paramagnetic resonance (EPR) was also carried out to verify the production of hydroxyl radicals using 5,5-dimethyl-1-pyrroline N-oxide (DMPO) as a ·OH-sensitive trapping agent.<sup>[25]</sup> The 1:1:1 triplet was only showed in E+Pt group, but not in the systems when only the AC field was applied or only PtNPs were added, reflecting that excess ROS was produced by PtNPs under the electric field (Figure S12, Supporting Information).<sup>[26]</sup>

Next, we would like to utilize the electro-driven ROS generation ability of PtNPs for cancer cell killing. First, we tested the cytotoxicity of PtNPs to mouse 4T1 breast tumor cells, using the standard methyl thiazolyl tetrazolium (MTT) cell viability assay (Figure 4a). After incubation with different concentrations of PtNPs for 24 h, no clear damage was observed to 4T1 cells even with the PtNPs' concentration up to  $200\text{ }\mu\text{g mL}^{-1}$ , demonstrating the in vitro biocompatibility of those nanoparticles.

To certify that PtNPs had the capability of causing cell damage under the electronic field, 4T1 cells were placed in a double salt bridges device and incubated with PtNPs for 2 h. After that, DC or square-wave AC with different duration time was imposed at the current of 5 mA for 10 min. Cell viabilities were measured after incubation for another 24 h (Figure 4b). While square-wave AC treatment (without PtNPs) even with the longest tested duration time (60 s) appeared to be safe to those cells, DC treatment on itself resulted in significant cell death, owing to the drastic pH changes nearby inserted electrodes. With the addition of PtNPs, the electro-driven cell death could be clearly enhanced. Consistent to the results in the MB degradation experiment (Figure 3c), square-wave AC with 60 s duration time was found to be the most effective in killing cancer cells in the presence of PtNPs. To compare side effect of electrodes and the range of cell killing effect, 4T1 cells seeded in 60 mm Petri dishes were treated with DC, 60 s AC (E), and 60 s AC plus PtNPs (E+Pt) by placing one electrode in the center of the Petri dishes at 5 mA for 10 min. Electrical circuit was formed by inserting a salt bridge at the side of Petri dish. Trypan blue was added following the incubation for another 12 h after the treatment. From the stained photographs of Petri dishes (Figure S13a–c, Supporting Information), it was clear

that DC treatment caused much more significant cell death in area nearby the centered electrodes compared to other two AC groups. Beyond the central zone with drastic pH variation induced by the inserted electrode, microscope images illustrated that more 4T1 cells were killed in areas far from the inserted electrode in the group with PtNP-based EDT (Figure S13d–f, Supporting Information), suggesting that EDT would resulted in a more uniform and extended cell-killing region.

Furthermore, 4T1 cells were incubated with the same concentration of PtNPs for different periods of time and then imposed to the 60 s square-wave AC at the flow current of 5 mA for 5 min. Cell viabilities were examined after incubation for further 24 h. It was found that, with the extension of incubation time, the EDT cell-killing effect increased continuously, indicating that the therapeutic effect in our system should be related to the presence of PtNPs inside cells (Figure S14, Supporting Information). We further tested the cell-killing effects under varied current flow and treatment time (Figure 4c; Figure S15, Supporting Information). PtNPs showed a decent level of therapeutic effect when treated with 60 s square-wave AC power supply at 5 mA for 10 min, which was the parameter used in the subsequent *in vitro* experiment.

After EDT treatment, live and dead cells were co-stained with Calcein-AM and propidium iodide (PI), which appeared in green and red, respectively, under a confocal fluorescence microscope (Figure 4d). Consistent with the cell viability assay data, incubation with PtNPs in the presence of 60 s square-wave AC resulted in the most apparent cell death. In addition, we evaluated the intracellular ROS generation via 2,7-dichlorodihydrofluorescein diacetate (DCFH-DA) fluorescence assay (Figure 4e). As expected, cells treated with PtNPs showed a higher level of ROS generation after 60 s square-wave AC treatment for 10 min. While mitochondrial membrane potential ( $\Delta\Psi_m$ ) is an indicator of cell apoptosis, JC-1 is a lipophilic, cationic dye that can selectively enter mitochondria and reversibly change color from green to red as the membrane potential increases in healthy living cells. Confocal fluorescence images (Figure 4f) and quantitative analysis data (Figure 4g) revealed that cells treated with PtNPs and 60 s square-wave AC showed much stronger green fluorescence and higher green-to-red ratio, indicating that the mechanism of cell damage in EDT was related to disturbed mitochondrial membrane potential. Moreover, the cell proliferation assay was evaluated by Ki-67 staining, which revealed the lowest number of proliferating cells for those with PtNPs' incubation and square-wave AC treatment (Figure S16, Supporting Information). Those results together evidenced that EDT treatment with PtNPs under 60 s square-wave AC would trigger effective production of intracellular ROS, which would trigger cell death and inhibit cell proliferation via mechanisms including disruption of mitochondrial membrane potential.

To evaluate the anticancer activity of PtNPs under square-wave AC power supply *in vivo*, the 4T1 tumor model was established on Balb/C mice. A total of 20 mice bearing 4T1 tumors at large initial sizes of  $\approx 500\text{ mm}^3$  were randomly divided into four groups ( $n = 5$  per group): untreated (Group 1), PtNPs injection only (Group 2), square-wave AC (Group 3), PtNPs' injection plus square-wave AC (Group 4). These mice were intratumor injected with PtNPs ( $50\text{ }\mu\text{L}, 2\text{ mg mL}^{-1}$ ) and treated with 60 s

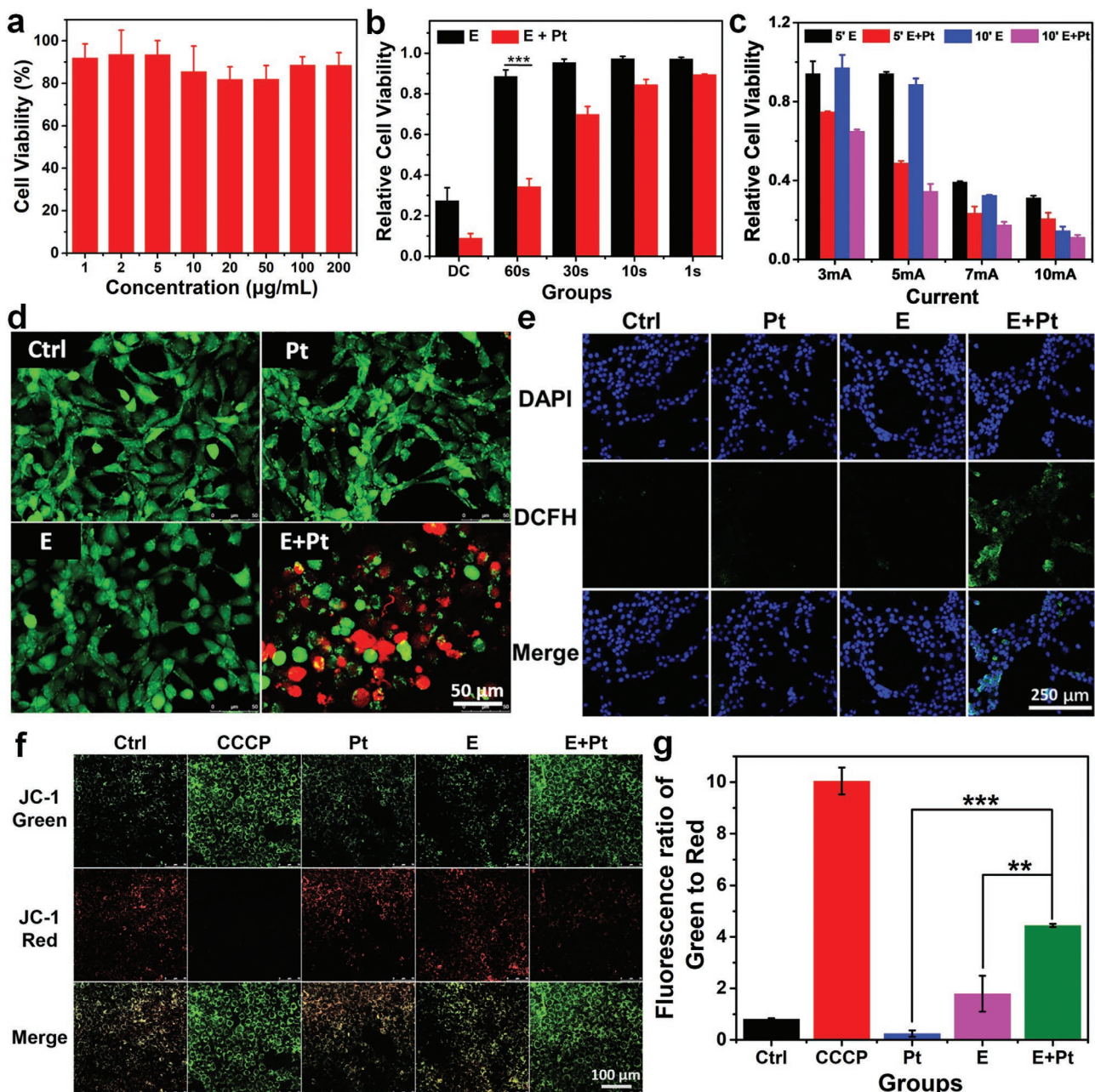


**Figure 4.** In vitro cell culture study. a) Relative viabilities of 4T1 cells after incubation with various concentrations of PtNPs for 24 h. b) Relative cell viability of electrodynamic-treated 4T1 cells under DC or square-wave AC (5 mA) with duration at 1, 10, 30, and 60 s for 10 min. c) In vitro electrodynamic treatment of 4T1 cells with different flow currents for 5 or 10 min under 60 s square-wave AC. d) Confocal fluorescence images of live (green) and dead (red) cells stained by Calcein-AM and PI after being treated with square-wave AC in the presence or absence of PtNPs. e) Intracellular ROS production of cells after different treatments using DCFH-DA as an ROS probe. f,g) Representative images and quantitative analysis of JC-1 stained cells after various treatments indicated. Carbonyl cyanide m-chlorophenyl hydrazone (CCCP) was used as a positive control.  $p$  values: \*\*\* $p < 0.001$ , \*\* $p < 0.01$ , \* $p < 0.05$ . Pt stands for PtNPs and E stands for square-wave AC electronic field.

square-wave AC power supply at 5 mA for 15 min. Wraparound electrodes insertion mode was used, with one circle electrode attached to the tumor boundary and the other inserted to the central area of the tumor (Figure 5a).

The tumor sizes and mice body weights were measured every 2 days after treatment (Figure 5b-d; Figure S17, Supporting Information). Tumor sizes of individual mouse from different

groups were recorded in detail until the mouse was dead or the tumor reached above  $2000 \text{ mm}^3$  (Figure 5d). It was found that PtNPs' injection plus square-wave AC treatment showed the most effective tumor growth suppression, while the same square-wave AC treatment or PtNPs injection alone showed no appreciable effect to the tumor growth (Figure 5b). After EDT treatment, tumors in the PtNP-based EDT group swelled and

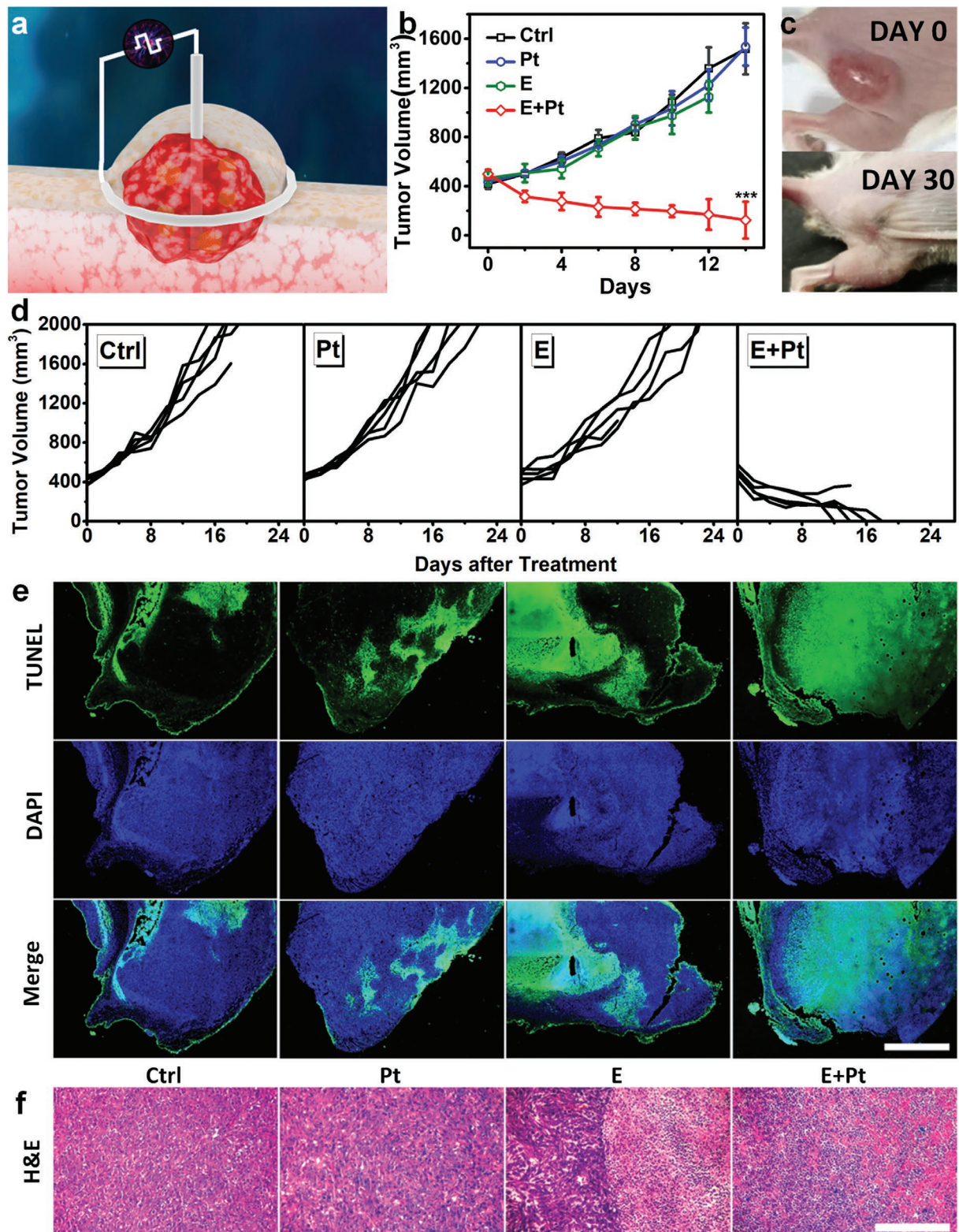


**Figure 5.** In vivo electrodynamic treatment effect. a) A scheme illustrating the tumor treatment process using wraparound electrodes. b) Average tumor volume growth curves of mice for the four different treatment groups ( $n = 5$  per group). c) Photographs of 4T1 tumor-bearing mice before and 30 days after EDT treatment with PtNPs. d) Tumor growth curves of individual mice various treatments indicated. e,f) Microscopic images of immunofluorescence e) TUNEL-stained (scale bar: 1 mm) and f) H&E stained (scale bar: 100  $\mu$ m) tumor slices collected from different groups of mice 24 h after treatment. Pt stands for PtNPs and E stands for square-wave AC electronic field.

turned dark immediately, and then shrank and hardened gradually overtime. About 16 days later, tumors became scabs and fell off. The skin wound was healed with  $\approx$ 30 days (Figure 5c). Representative photographs of one mouse from each group of mice taken at various time points after different treatment were shown in Figure S18 (Supporting Information).

To further confirm the *in vivo* tumor destruction effect, immunofluorescence terminal deoxynucleotidyl transferase-mediated dUTP-biotin nick end labeling (TUNEL) stained confocal mosaic images of tumor slices, which were sectioned 24 h after treatment, were shown in Figure 5e. Only small proportions of tumors showed apoptotic signals for those in the untreated group and PtNPs' injected group. For tumors with electrodes inserted and treated by 60 s square-wave AC (no PtNPs' injection), a half of those tumors showed apoptotic signals. In contrast, a large scale of apoptosis was found for the entire tumor after EDT treatment with PtNPs. Similar trend was also found for hematoxylin and eosin (H&E)-stained tumor slices, which demonstrated that cells were largely damaged in the group with PtNPs injection and square-wave AC treatment (Figure 5f). Therefore, our results suggest that EDT treatment with PtNPs or other nanoparticles with electro-driven ROS generation abilities is an effective approach for local elimination of large solid tumors. Further studies in large animal models with larger tumors are still needed to further demonstrate the potential superiority of EDT over conventional EChT for tumor treatment.

It is noteworthy that, comparing to other ROS-based therapeutic approaches, so-called "dynamic therapy" (e.g., PDT, SDT, CDT, and RDT), EDT by decomposing water molecules under the action of electric field to produce hydroxyl radicals, would offer a series of unique advantages. In "dynamic therapies" such as PDT, SDT, or RDT, ROS are produced from oxygen molecules under the action of the external field (e.g., light, ultrasound, or radio).<sup>[12b,14a,15]</sup> However, the hypoxic characteristics of tumor microenvironment would significantly limit the production of ROS and thus hamper the efficacy of those "dynamic therapies." In addition, CDT, which relies on *in situ* reactions in the tumor region, is highly dependent to the substance in the complex tumor microenvironment, such as  $H_2O_2$  and  $H^+$ .<sup>[16b]</sup> The reactant source could be limited for generating ROS in a lasting manner.

In summary, we have proposed a new electric stimulation modality, EDT, for cancer therapy through electro-driven catalytic reaction of PtNPs in the square-wave AC electric field. Based on the experimental verification and computational simulation, we demonstrated that PtNPs have the ability to catalyze water molecule decomposition to produce ROS in the presence of chlorine ions. This mechanism induces the death of cancer cells and could be employed for local ablation of solid tumors. In addition to PtNPs, other types of noble metal-based nanocatalysts are also expected to be explored for EDT. Unlike the traditional EChT, EDT utilizes a new mechanism for ROS generation to kill tumor cells, similar to other types of "dynamic therapies." This EDT mechanism significantly enhances tumor-killing specificity and mitigates side effects to normal tissues, and allows its effective treatment of hypoxic tumors. Compared to the conventional EChT, EDT is much less invasive with significantly reduced damages to tissues nearby

the inserted electrodes, and could be applied for homogeneous destruction of large tumors without the need of cumbersome electrode design. Furthermore, this EDT therapeutic approach may be feasibly combined with other therapeutic protocols for enhanced cancer treatment in future studies. This study therefore offers a brand new category of tumor therapy technology, and may spark a series of follow-on explorations in the area of nanomedicine.

## Supporting Information

Supporting Information is available from the Wiley Online Library or from the author.

## Acknowledgements

This work was financially supported by the National Nature Science Foundation of China (Grant Nos. 51672247, 51525203, 51572180), the 111 program of China (Grant No. B16042), and the National Research Programs from Ministry of Science and Technology (MOST) of China of China (2016YFA0201200, 2016YFC1101900) and the Collaborative Innovation Center of Suzhou Nano Science and Technology.

## Conflict of Interest

The authors declare no conflict of interest.

## Keywords

electrochemical therapy (EChT), hydroxyl radicals, platinum nanoparticles, square-wave alternating current, tumor therapy

Received: October 20, 2018

Revised: January 25, 2019

Published online: February 8, 2019

- [1] a) E. Nilsson, H. V. Euler, J. Berendson, A. Thörne, P. Wersäll, I. Näslund, A. S. Lagerstedt, K. Narfström, J. M. Olsson, *Bioelectrochemistry* **2000**, 51, 1; b) E. Cabuy, *Electrochemical Therapy in Cancer Treatment*, University of Ljubljana, Slovenia **2012**.
- [2] C. Holandino, C. A. Teixeira, F. A. de Oliveira, G. M. Barbosa, C. M. Siqueira, D. J. Messeder, F. S. de Aguiar, V. F. da Veiga, W. Girard-Dias, K. Miranda, A. Galina, M. A. Capella, M. M. Morales, *Bioelectrochemistry* **2016**, 111, 83.
- [3] a) L. E. B. Cabrales, J. I. Montijano, M. Schonbek, A. R. S. Castañeda, *Math. Comput. Simul.* **2018**, 151, 96; b) E. Nilsson, E. Fontes, *Bioelectrochemistry* **2001**, 53, 213.
- [4] a) J. H. Li, Y. L. Xin, X. Q. Fan, J. Chen, J. Wang, J. Zhou, *Chin. J. Integr. Med.* **2013**, 19, 387; b) H. V. Euler, E. Nilsson, J. M. Olsson, A. S. Lagerstedt, *Bioelectrochemistry* **2001**, 54, 117.
- [5] a) D. Miklavčič, G. Serša, M. Kryžanowski, S. Novakovič, F. Bobanović, R. Golouh, L. Vodovnik, *Bioelectrochem. Bioenerg.* **1993**, 30, 11; b) L. B. Cabrales, H. C. Ciria, R. P. Bruzón, M. S. Quevedo, R. H. Aldana, L. M. D. Oca, M. F. Salas, O. G. Peña, *Bioelectromagnetics* **2010**, 22, 6.
- [6] a) L. Jing-Hong, X. Yu Ling, *Conf. Pap. Med.* **2013**, 2013, 1; b) H. von Euler, J. M. Olsson, K. Hultenby, A. Thörne, A.-S. Lagerstedt, *Bioelectrochemistry* **2003**, 59, 89.

- [7] A. R. Aguilera, L. E. B. Cabrales, H. M. C. Ciria, Y. S. Pérez, E. R. Oria, S. A. Brooks, T. R. González, *Math. Comput. Simul.* **2009**, *79*, 2091.
- [8] a) M. Telló, L. Oliveira, O. Parise, A. C. Buzaid, R. T. Oliveira, R. Zanella, A. Cardona, *Conf. IEEE Eng. Med. Biol. Soc.* **2007**, *2007*, 3524; b) Y. Belyy, A. Tereshchenko, A. Shatskikh, *Ecancermedical-science* **2012**, *6*, 272.
- [9] a) X. Sun, B. Yuan, W. Rao, J. Liu, *Biomaterials* **2017**, *146*, 156; b) F. L. Cury, B. Bhindi, J. Rocha, E. Scarlata, K. El Jurdì, M. Ladouceur, S. Beauregard, A. K. Vijh, Y. Taguchi, S. Chevalier, *Bioelectrochemistry* **2015**, *104*, 1.
- [10] a) L. S. Lin, J. Song, L. Song, K. Ke, Y. Liu, Z. Zhou, Z. Shen, J. Li, Z. Yang, W. Tang, G. Niu, H. H. Yang, X. Chen, *Angew. Chem., Int. Ed.* **2018**, *57*, 4902; b) J. Herman, Y. Zhang, V. Castranova, S. L. Neal, *Anal. Bioanal. Chem.* **2018**, *410*, 6079; c) X. Zhen, K. Pu, *Nano Res.* **2018**, *11*, 5258.
- [11] a) D. K. Deda, K. Araki, *J. Braz. Chem. Soc.* **2015**, *26*, 2448; b) J. Wei, J. Li, D. Sun, Q. Li, J. Ma, X. Chen, X. Zhu, N. Zheng, *Adv. Funct. Mater.* **2018**, *28*, 1706310.
- [12] a) D. Costley, C. Mc Ewan, C. Fowley, A. P. McHale, J. Atchison, N. Nomikou, J. F. Callan, *Int. J. Hyperthermia* **2015**, *31*, 107; b) L. Serpe, F. Foglietta, R. Canaparo, *Nano Rev.* **2012**, *1*, 173.
- [13] a) C. Zhang, W. Bu, D. Ni, S. Zhang, Q. Li, Z. Yao, J. Zhang, H. Yao, Z. Wang, J. Shi, *Angew. Chem., Int. Ed.* **2016**, *55*, 2101; b) Z. Tang, H. Zhang, Y. Liu, D. Ni, H. Zhang, J. Zhang, Z. Yao, M. He, J. Shi, W. Bu, *Adv. Mater.* **2017**, *29*, 1701683.
- [14] a) K. Lu, C. He, N. Guo, C. Chan, K. Ni, G. Lan, H. Tang, C. Pelizzari, Y.-X. Fu, M. T. Spiotto, R. R. Weichselbaum, W. Lin, *Nat. Biomed. Eng.* **2018**, *2*, 600; b) J. Takahashi, M. Murakami, T. Mori, H. Iwahashi, *Sci. Rep.* **2018**, *8*, 2728.
- [15] Z. Zhou, J. Song, L. Nie, X. Chen, *Chem. Soc. Rev.* **2016**, *45*, 6597.
- [16] a) M. Ferrari, *Nat. Rev. Cancer* **2005**, *5*, 161; b) H. Lin, Y. Chen, J. Shi, *Chem. Soc. Rev.* **2018**, *47*, 1938.
- [17] a) M. Moglianetti, E. De Luca, D. Pedone, R. Marotta, T. Catelani, B. Sartori, H. Amenitsch, S. F. Retta, P. P. Pompa, *Nanoscale* **2016**, *8*, 3739; b) L. Zhang, L. Laug, W. Munchgesang, E. Pippel, U. Gosele, M. Brandsch, M. Knez, *Nano Lett.* **2010**, *10*, 219; c) U. Carmona, L. Zhang, L. Li, W. Munchgesang, E. Pippel, M. Knez, *Chem. Commun.* **2014**, *50*, 701.
- [18] a) D. Pedone, M. Moglianetti, E. De Luca, G. Bardi, P. P. Pompa, *Chem. Soc. Rev.* **2017**, *46*, 4951; b) H. Wei, E. Wang, *Chem. Soc. Rev.* **2013**, *42*, 6060.
- [19] a) T. Teranishi, M. Miyake, M. Hosoe, *Adv. Mater.* **1997**, *9*, 65; b) T. Teranishi, M. Miyake, *Chem. Mater.* **1998**, *10*, 594.
- [20] a) J. S. Lee, K. H. You, C. B. Park, *Adv. Mater.* **2012**, *24*, 1084; b) Y. Tang, W. Di, X. Zhai, R. Yang, W. Qin, *ACS Catal.* **2013**, *3*, 405.
- [21] a) B. Hammer, J. K. Norskov, *Nature* **1995**, *376*, 238; b) Z. Zhao, C. Chiu, J. Gong, *Chem. Sci.* **2015**, *6*, 4403.
- [22] J. H. Hao, R. Jiang, Y.-H. Yin, Y.-F. Wang, Q.-H. Jin, *Surf. Sci.* **2013**, *617*, 233.
- [23] G. Makov, M. C. Payne, *Phys. Rev. B* **1995**, *51*, 4014.
- [24] K. Setsukinai, Y. Urano, K. Kakinuma, H. J. Majima, T. Nagano, *J. Biol. Chem.* **2003**, *278*, 3170.
- [25] G. M. Pieper, C. C. Felix, B. Kalyanaraman, M. Turk, A. M. Roza, *Free Radical Biol. Med.* **1995**, *19*, 219.
- [26] J. M. Fontmorin, R. C. Burgos Castillo, W. Z. Tang, M. Sillanpää, *Water Res.* **2016**, *99*, 24.